Journal of Thermal Analysis and Calorimetry (2019) 138:1081–1095
https://doi.org/10.1007/s10973-019-08262-0

Non-isothermal crystallization kinetics and nucleation behavior of isotactic polypropylene composites with micro-talc

Abdelheq Layachi[1,2] · Azzedine Makhlouf[2,3] · Djamel Frihi[4] · Hamid Satha[2] · Ahmed Belaadi[2,5] · Roland Seguela[6,7]

Received: 7 November 2018 / Accepted: 15 April 2019 / Published online: 30 April 2019

Abstract

The non-isothermal crystallization (NIC) of isotactic polypropylene (iPP) and its composites with submicronic talc particles (μ-talc) was investigated by differential scanning calorimetry. The modeling of the NIC kinetics of the iPP matrix was performed using Jeziorny-modified Avrami's model, Ozawa's and Mo's theoretical approaches. The Jeziorny's and Ozawa's theories allowed us to confirm that the μ-talc filler particles significantly promote the NIC kinetics of the iPP matrix which noticeably manifests itself via a change in the nucleation mechanism. However, Mo's model proved to be the more relevant model to account for the NIC of the present materials. In parallel, the activation energy and nucleation activity of NIC were calculated by Kissinger's and Dobreva's methods, respectively. Both approaches reveal that a maximum nucleation activity of μ-talc takes place for 20% filler content. This finding is discussed in relation to the μ-talc content thresholds of mechanical percolation and crystallinity saturation that were reported in previous studies for these composites, about 10 and 30% μ-talc, respectively. An endeavor of physical explanation for these phenomena is put forward.

Keywords Polypropylene · Talc · Composite · DSC · Crystallization kinetics · Nucleation activity

Introduction

Polypropylene (PP) is one of the most common semicrystalline thermoplastics to be used in the industry owing to its good mechanical properties [1], the possible treatment, good impact resistance, high stiffness and a low thermal expansion coefficient. Minerals fillers and synthetic as well as natural fibers are largely prevalent in industrial applications for manufacturing polymer-based composites [2–7] as they enable reducing the cost and improving the thermo-mechanical performances of composites based on various polymer matrices, and particularly PP [2]. Mineral fillers are also known to often improve the crystallization of semicrystalline polymers, particularly PP. These filler-induced properties are, however, strongly dependent on the degree of dispersion on the filler in the polymer matrix.

Among mineral fillers available for the mechanical reinforcement of PP-based composites, calcium carbonate and short glass fibers have been the subject of much research [8–15]. In recent years, talc has proven to have a high potential of development for the reinforcement of PP-

✉ Abdelheq Layachi
abdelhak2416@live.fr

✉ Hamid Satha
sathahamid@yahoo.fr

1 Institut des Sciences et Techniques Appliquées, UFMC 1, 25000 Constantine, Algeria

2 Laboratoire des Silicates, Polymères et Nanocomposites, Université du 8 Mai 1945, 24000 Guelma, Algeria

3 Université Abbès Laghrour, 40000 Khenchela, Algeria

4 Université du 8 Mai 1945, 24000 Guelma, Algeria

5 Université du 20 aout 1955, 21000 Skikda, Algeria

6 MATEIS, UMR CNRS 5510, INSA de Lyon, Bât. Blaise Pascal, 69621 Villeurbanne, France

7 Univ Lyon, Campus LyonTech - La Doua, 69621 Villeurbanne, France

based composites [11–25], essentially for manufacturing parts in the automotive industry, leisure furniture, home appliances, etc. It soon became obvious that talc exhibits a strong nucleation effect in the PP matrix due to specific physicochemical interactions between the filler and the polymer matrix that promote crystallization.

In the last three decades, considerable interest has been addressed to polymer-based nanocomposites with clay-like fillers [26, 27], including PP-based nanocomposites [28–30], owing to the spectacular mechanical effect of clay particles having nanometric size and high form factor. This finding incited mineral filler manufacturers to develop nanofillers from conventional ones such as calcium carbonate or talc in view of improving the mechanical performances of filler-reinforced polymers [31–38].

Branciforti et al. [24] investigated the effect of different concentrations of fine talc powder on the molecular orientation and crystallinity of the PP matrix of injection-molded PP-talc composites. It was found that the presence of talc particles in the composites involves a strong influence on the crystallinity of the PP matrix that levels-off beyond 20 mass% of talc content. This effect was markedly greater than that observed for other mineral fillers such as calcium carbonate or kaolin, which resulted in a better improvement of the mechanical properties [13]. Moreover, the specific physicochemical interactions between talc particles and the iPP matrix make talc to be easily incorporated in PP without the use of a surface treatment [39], though the use of such treatment has been reported to be an efficient means for talc particle dispersion in polymer matrix. Another significant advantage of talc over calcium carbonate or kaolin from a practical point of view is that it is much less abrasive for the extruder during mixing and injection molding [13, 15].

In a parallel study of the mechanical properties of iPP composites with submicronic talc, namely μ-talc, Frihi et al. [40] revealed the occurrence of a mechanical percolation network between the iPP crystalline lamellae and the μ-talc platelets at low filler loading. The saturation threshold of this phenomenon occurred at μ-talc content about 10% by mass. It was also shown that μ-talc provides significantly higher stiffness and yield stress as well to the iPP composites than conventional talc at equivalent filler loading.

More recently, Makhlouf et al. [41] investigated the same iPP composites from the standpoint of crystallization potentiality, i.e., the effects of μ-talc content and cooling rate. It was found that μ-talc strongly promotes the crystallinity of the iPP matrix as judged by its significant increase with increasing μ-talc content. In agreement with Branciforti et al. [24], Makhlouf et al. also observed a tendency to saturation of the iPP crystallinity for μ-talc content beyond 20%. Makhlouf et al. argued that this phenomenon arose from the crowding of the μ-talc platelets with increasing FR which disrupt the growth of iPP crystalline lamellae. This interpretation borrows from Fornes and Paul [42] and Lincoln et al. [43] who observed similar phenomena for nylon6–clay nanocomposites.

Considering that the physical and mechanical properties of semicrystalline polymers are governed by the morphology of the material is essential to investigate the crystallization behavior. Crystallization is particularly non-isothermal during the processing of the material into useful parts. Therefore, the study of non-isothermal crystallization (NIC) kinetics is a major issue for understanding and optimizing the useful properties of the polymer and its composites as well. In the last two decades, various theoretical approaches borrowed from Avrami [44–46], Jeziorny [47], Ozawa [48] and Mo [49–51] have been used to account for the NIC kinetics of polypropylene filled with conventional talc powders. The present paper reports on the use of the above-mentioned approaches for studying the NIC kinetics of the iPP/μ-talc composites in order to get a better insight on the nucleation efficiency of μ-talc on the iPP matrix.

This study is complementary to the previous one [41] dealing with the optimization of the crystallinity ratio under NIC conditions. For this objective, experiments were conducted by differential scanning calorimetry on a series iPP/μ-talc composites containing various concentrations of μ-talc up to 30% by mass. The present work focuses on the crystallization kinetics and nucleation activity of μ-talc particles in these composites. The novelty lies in the evidence of a saturation effect of μ-talc on its nucleation activity at a lower concentration than the saturation thresholds of the crystallinity ratio and the mechanical percolation as well, as previously reported.

Experimental methods

Materials and processing

The isotactic polypropylene (iPP) with an isotacticity index of 96% was supplied by Solvay (Brussels, Belgium). Its mass-average molar mass was $M_w \approx 380$ kg mol^{-1} and its polydispersity index IP ≈ 12. The study was carried out on iPP composites reinforced with a submicronic size talc powder under trade name HAR®Talc (High Form factor Talc) from Imerys Talc Luzenac (France) without surface treatment, hereafter designated as μ-talc. The specific surface area of the present μ-talc powder was 17 m^2 g^{-1} as determined by the Brunauer–Emmett–Teller method, according to the manufacturer. The average thickness of the μ-talc platelets was 0.39 μm with a

standard deviation of 0.13 μm and their average form factor was 5.5 as measured by scanning electron microscopy [40].

All the composites containing 5%, 10%, 20% and 30% by mass of μ-talc, denoted filler content FR, were compounded by Multibase/Dow Corning (Saint-Laurent-du-Pont, France) without any compatibilizing agent, using a Clextral BC21 twin screw extruder of length 1200 mm and diameter 25 mm, with a regulation temperature range 180–210 °C between the feeder and the die. The composites were finally injection-molded into 2 mm thick sheets. Neat iPP was also processed following the same procedure. More details on the processing conditions are provided elsewhere [41].

Characterization methods

Differential scanning calorimetry (DSC) was used to study the NIC of neat iPP and its μ-talc composites. The apparatus was a DSC7 from Perkin Elmer using samples of about 10 mg and various cooling rates, CR, namely 5, 10, 15 and 20 °C min^{-1}, in the temperature range 200–25 °C. The ovens were purged with dried nitrogen at a flux rate of about 20 mL min^{-1}. The temperature scale was calibrated upon heating at every rate using high purity indium. The relative crystallinity as a function of temperature during crystallization, $X(T)$, was computed from the following relation for all composites and neat iPP

$$X(T) = \frac{\int_{T_0}^{T} (\mathrm{d}H_C/\mathrm{d}T)\mathrm{d}T}{\int_{T_0}^{T_\infty} (\mathrm{d}H_C/\mathrm{d}T)\mathrm{d}T} \quad (1)$$

where T_o and $T_\propto$ hold for the temperature onset and final temperature of the crystallization exotherm, respectively, and dH_c/dT is the incremental heat flux of crystallization as measured from the DSC recordings at every cooling rate. Also were recorded the experimental data of crystallization temperature at the peak of the crystallization exotherm, T_c, and crystallization half time, $t_{1/2}$, for neat iPP and composites. It is worth noticing that the absolute values of the crystallinity of the various materials have been reported in a previous paper [41].

For the sake of identifying the crystalline form of the iPP matrix, the melting behavior of neat iPP and all iPP/μ-talc composites was recorded from the DSC heating scans at a heating rate of 10 °C min^{-1}.

Wide-angle X-ray scattering (WAXS) experiments were carried out at room temperature in transmission mode on a laboratory bench using a rotating Cu-anode from Rigaku (Tokyo, Japan) operated at 100 kV and 40 mA. The X-ray beam was collimated with Göbel mirrors from Xenocs (Grenoble, France) providing a monochromatic Cu-Kα radiation of wavelength 0.154 nm together with parallel point focusing thanks to 2 pairs of anti-scattering slits. The 2D-WAXS patterns were recorded on a SCX2D-CCD camera from Princeton Instruments (Trenton NJ, USA). More details on the experimental procedure are given elsewhere [41].

Experimental results

The edge-view WAXS intensity profiles of Fig. 1 reveal the presence only of the crystalline α-phase of iPP in both the neat iPP sample and the iPP/10% μ-talc/composite. All composites not shown here also exhibit the α-phase crystalline phase only. This structural feature is quite useful for the present study in the aim of a global approach of the crystallization kinetics of this system since the occurrence of two crystalline phases would have involved a complex analysis. This structural habit of the present iPP/μ-talc composites is corroborated by the DSC melting curves of Fig. 2 that clearly disclose a single melting endotherm relevant to the α-crystal form only for all the composites and neat iPP as well. Useful comparison can be made with iPP-based materials displaying both the α and the β crystalline forms [52, 53].

It is also worth noticing from Fig. 1 that, though both neat iPP and iPP/10% μ-talc composite display the same characteristic reflections of the iPP α-crystal form, the composite does not exhibit the predicted intensity of these characteristic reflections, i.e., the (040) reflection is surprisingly prominent. As already pointed out in the previous study [41], this is relevant to a processing-induced texturing effect that entails a preferred orientation of the chains

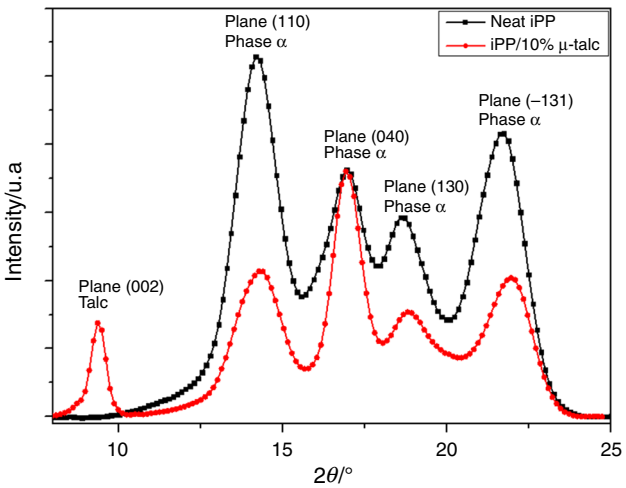

Fig. 1 Edge-view WAXS intensity profiles of neat iPP and iPP/10%μ-talc composite

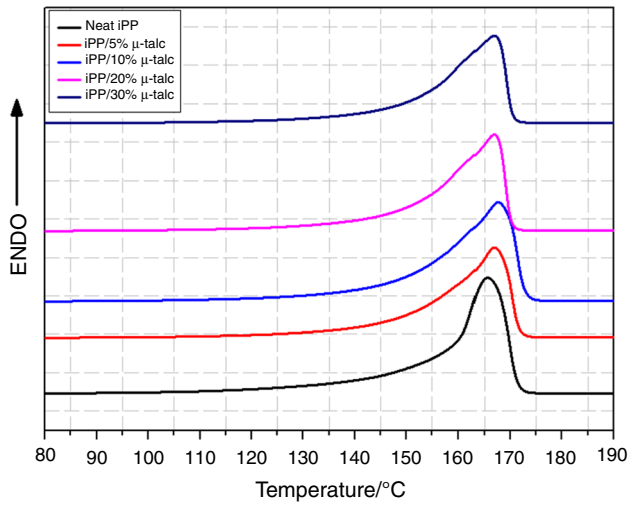

Fig. 2 Melting curves of neat iPP and iPP/μ-talc composites

in the main plane of the injection-molded sheet involving a stronger intensity of the (040) reflection compared to other ones. In parallel, the presence of the (002) characteristic reflection of talc is also relevant to the preferred orientation of the talc platelets within the sample plane as previously observed via transmission electron microscopy [40]. All the other composites display similar texture characteristics. This structural feature will be later reminded in "Concluding discussion" section regarding the nucleation activity of μ-talc.

The curves of NIC recorded for the four cooling rates are reported in Fig. 3 for neat iPP and all composites. As usually observed, the crystallization exotherm globally shifts to lower temperature with increasing cooling rate for all materials. The data of peak crystallization temperature, T_c, reported in Table 1 confirm this observation that is relevant to the kinetic character of the process. However,

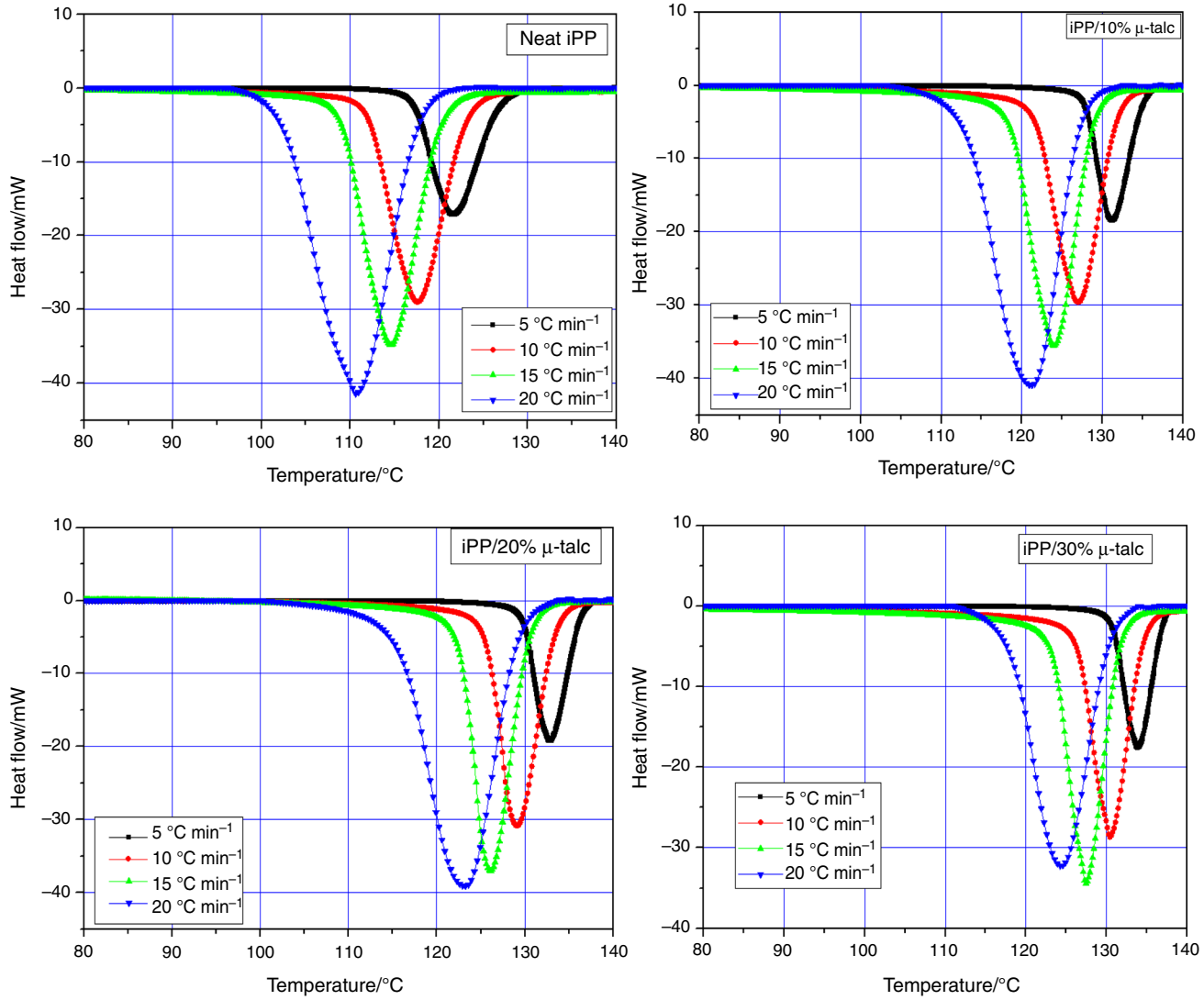

Fig. 3 Non-isothermal crystallization exotherms of neat iPP and iPP/μ-talc composites

Table 1 Crystallization temperature, T_c, and crystallization half time, $t_{1/2}$, data for NIC of neat iPP and iPP/μ-talc composites at various cooling rates, CR

Sample	CR/°C min^{-1}	T_c/°C	$t_{1/2}$/min
neat iPP	5	121.6	1.14
	10	117.6	0.67
	15	114.5	0.44
	20	110.6	0.36
iPP/5% μ-talc	5	130.5	0.85
	10	126.5	0.62
	15	123.5	0.41
	20	120.6	0.37
iPP/10% μ-talc	5	131.2	0.88
	10	127.0	0.57
	15	124.0	0.38
	20	121.3	0.34
iPP/20% μ-talc	5	132.8	0.75
	10	129.1	0.45
	15	126.1	0.31
	20	123.3	0.27
iPP/30% μ-talc	5	133.8	0.73
	10	130.5	0.49
	15	127.5	0.34
	20	124.3	0.32

T_c is systematically higher for the composites at any cooling rate, and the higher is the μ-talc content the higher is T_c.

This result indicates that μ-talc promotes the crystallization of the iPP matrix via a nucleation effect onto the surface of the μ-talc platelets. This nucleation effect is responsible for the macroscopic crystalline texturing of the iPP matrix in the injection-molded sheets of the composites owing to the shear-induced orientation of the μ-talc platelets, as already pointed out in the previous study regarding the same composites [41].

The variation during cooling of the melt-to-crystal transformation ratio, namely the relative crystallinity, is reported in Fig. 4 as a function of temperature for all the materials. Every curve displays the common sigmoidal shape relevant to three regimes of the crystallization process. The low slope of the curve at the beginning of the transformation arises from the necessary time for generating a sufficient number of nuclei before crystal growth could start, i.e., the nucleation-dominated regime. The intermediate stationary stage with a nearly constant and high slope corresponds to the actual growth of the crystals, i.e., the crystal growth-dominated regime. At the final stage of the transformation, the amount of untransformed material turns lower and lower so that the production of new nuclei as well as the growth crystallites drop and finally stop, i.e., the crystallization completion.

The curves of Fig. 4 are just another view of the DSC plots of Fig. 3 thanks to their normalized integration. At constant cooling rate, the gradual shift to higher temperature of the curves with the increase in μ-talc content confirms the nucleation effect of the μ-talc particles on the global crystallization the iPP matrix.

Transformation of the X_c data from temperature to time dependence is carried out thanks to the next relation

$$t = (T_o - T)/\mathrm{CR} \quad (2)$$

where t is the crystallization time, T_o is the crystallization temperature onset and CR is the cooling rate. Plots of the relative crystallinity variations with time, $X_c(t)$, are shown in Fig. 5 for neat iPP and composites for the various cooling rates. All the curves exhibit a similar sigmoidal shape. As cooling rate increases, the curves are shifted to shorter times. At constant cooling rate, the curves shift to shorter time with increasing μ-talc content.

The half-time crystallization, $t_{1/2}$, obtained for $X_c(t) = 50\%$ from Fig. 5, are reported in Table 1. For any constant cooling rate, the $t_{1/2}$ values are lower for all composites compared to neat iPP, i.e., μ-talc particles definitely act as nucleating and accelerating agents on the overall crystallization process of the iPP matrix. However, for every composite, the $X(t)$ curves at cooling rate CR = 30 °C min^{-1} are very close to the ones at CR= 20 °C min^{-1} which suggests that the potential nucleation activity of μ-talc is reduced at high cooling rates. Moreover, at any cooling rate, $t_{1/2}$ gradually drops with increasing μ-talc content up to FR = 20% then slightly increases for FR= 30%. On the one hand, this finding corroborates the μ-talc nucleation activity previously observed from the T_c evolution as a function of μ-talc content, but on the other hand, it clearly suggests that too much μ-talc particles are likely to hinder the growth of the iPP crystallites lamellae.

Analysis of non-isothermal crystallization kinetics

There are a number of kinetic models such as Avrami's, Ozawa's and Mo's approaches that can be applied for describing the NIC behavior of polymers. In the next section, all these approaches are tested in order to determine the most appropriate one to account for the crystallization of iPP in the present iPP/μ-talc composites.

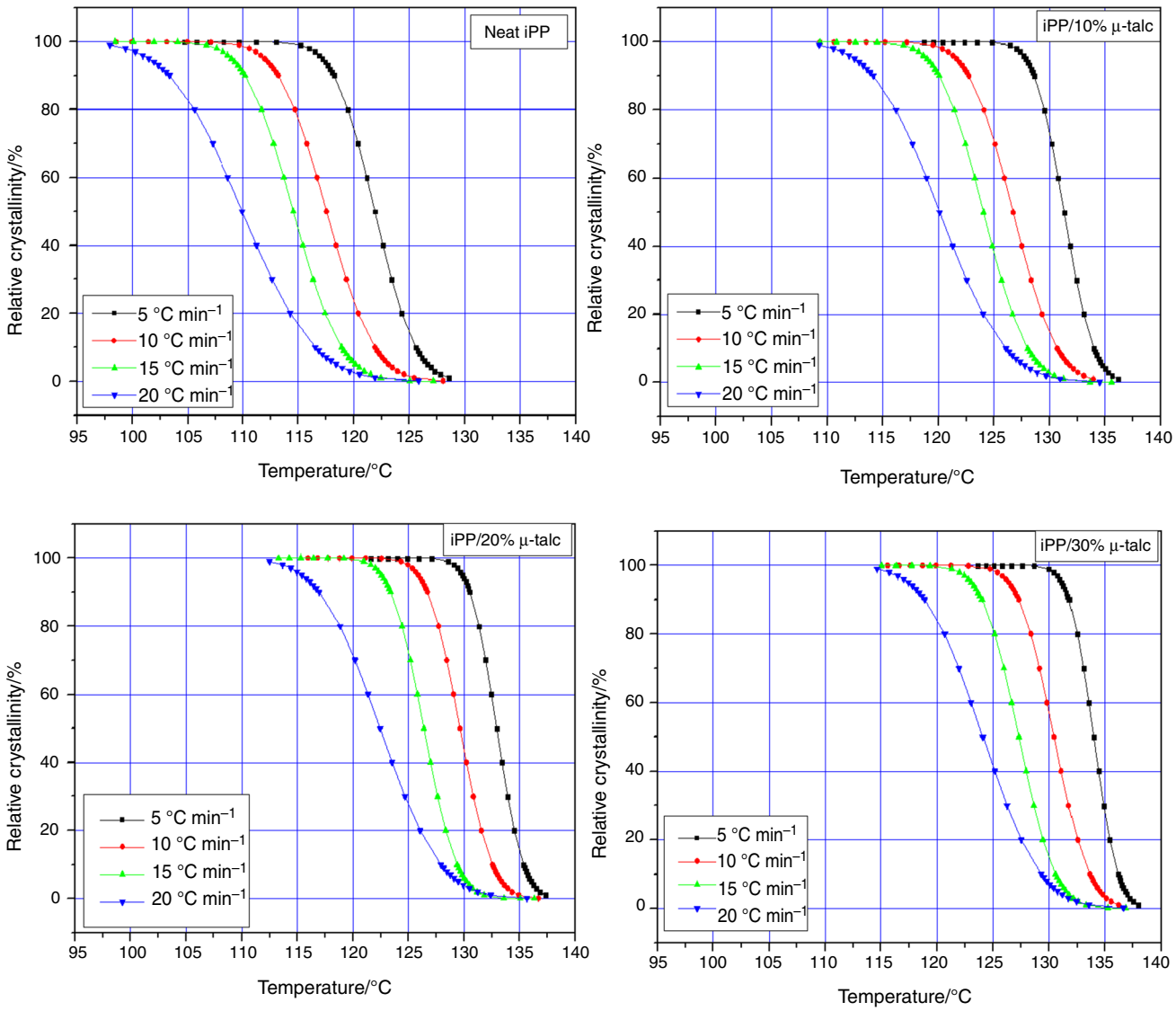

Fig. 4 Relative crystallinity as a function of temperature for neat iPP and iPP/μ-talc composites at different cooling rates

Avrami's theory modified by Jeziorny

Avrami's approach [44, 45] is often used to analyze the isothermal crystallizations behavior of polymer via the following relationship

$$1 - X(t) = \exp(-Zt^{n}) \tag{3}$$

that can be changed for a practical use into the next equation

$$\log[-\ln(1 - X(t))] = \log Z + n \log t \tag{4}$$

A plot of log $[-\ln(1 - X(t)]$ versus log t is typically linear in the range $0.2 \leq X(t) \leq 0.8$ and yields the Avrami's parameters Z and n via the intercept and the slope of the linear plot, respectively.

To account for NIC conditions, Jeziorny [46, 47] modified the Z parameter by introducing the cooling rate CR, as $\log Z_c = \log Z/\mathrm{CR}$. Figure 6 shows the log [ln (1 − X(t))] evolution versus log t for neat iPP and composites at different cooling rates.

Jeziorny's parameters computed from the data of Fig. 6 are reported in Table 2. The geometric n parameter does not display clear evolution trends with μ-talc content and cooling rate as well. In contrast, Z_c increases with cooling rate indicating that the transformation rate increases in parallel. The most striking finding from the data of Table 2 is that, except for the lowest cooling rate (within the experimental accuracy), Z_c increases with μ-talc content up to FR = 20% before to display a slight decrease. This finding is perfectly consistent with the previous observation regarding the evolution of the $t_{1/2}$ parameter with μ-talc

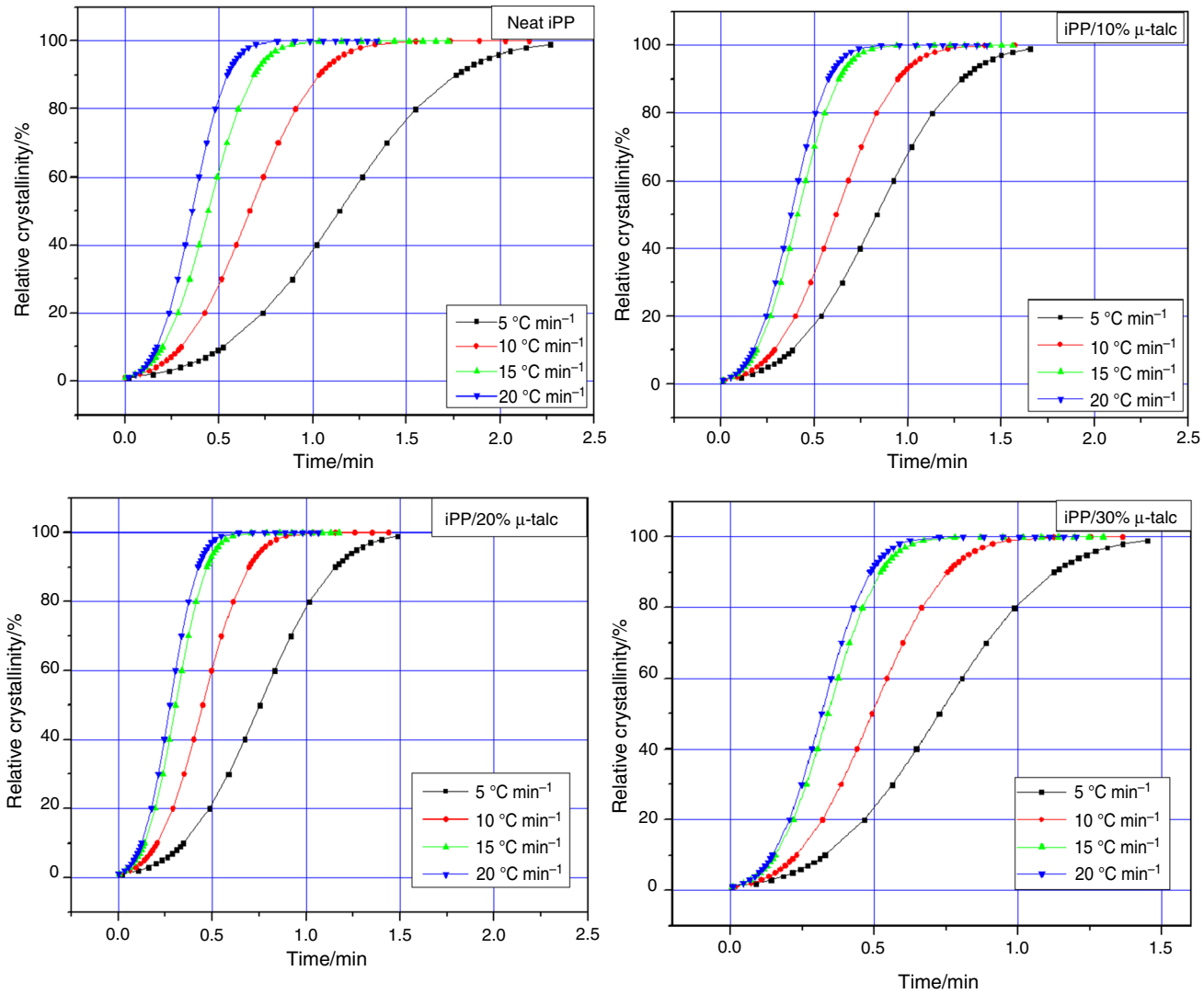

Fig. 5 Relative crystallinity as a function of time for neat iPP and iPP/μ-talc composites at different cooling rates

content. Both findings suggest the occurrence of a saturation effect in the nucleation activity of μ-talc on the crystallization of iPP. This point will be further argued in "Concluding discussion" section.

Ozawa's model

The results obtained from the NIC of the materials under investigation in the study were compared with the Ozawa's theory [48], which makes it possible to quantify by means of Avrami's coefficient m the type of nucleation, that may be homogeneous or heterogeneous, and the growth geometry. This theory is an extension of that of Avrami that applies in the case of isothermal crystallization. The characterization of the type of nucleation by Ozawa's method obeys the following Eq. (5)

$$\log[-\ln(1 - X(T)] = \log K(T) - m\log(\mathrm{CR}) \quad (5)$$

where $X(T)$ is the relative crystallinity depending on temperature T and cooling rate CR, and $K(T)$ is the temperature function and m is the Ozawa's exponent.

In Eq. (5), the term log $[-\ln(1 - X(T)]$ depends linearly on the entity log CR at a given crystallization temperature. To obtain the traces from the Ozawa's theory, a range of temperature validity must be taken into account for each peak of crystallization. The kinetic constants log $K(T)$ and m are estimated, respectively, from the intersection and the slope of the curve of log $[\ln (1 - X(T))]$ versus log CR are reported in Table 3 from the plots of Fig. 7. Whether a clear evidence of an improved crystallization kinetics of the composites appears with the increase in μ-talc content, in contrast the evolution of the m parameter does not display a clear tendency regarding the modification of crystal growth morphology. Any attempt for a morphological interpretation would be highly speculative.

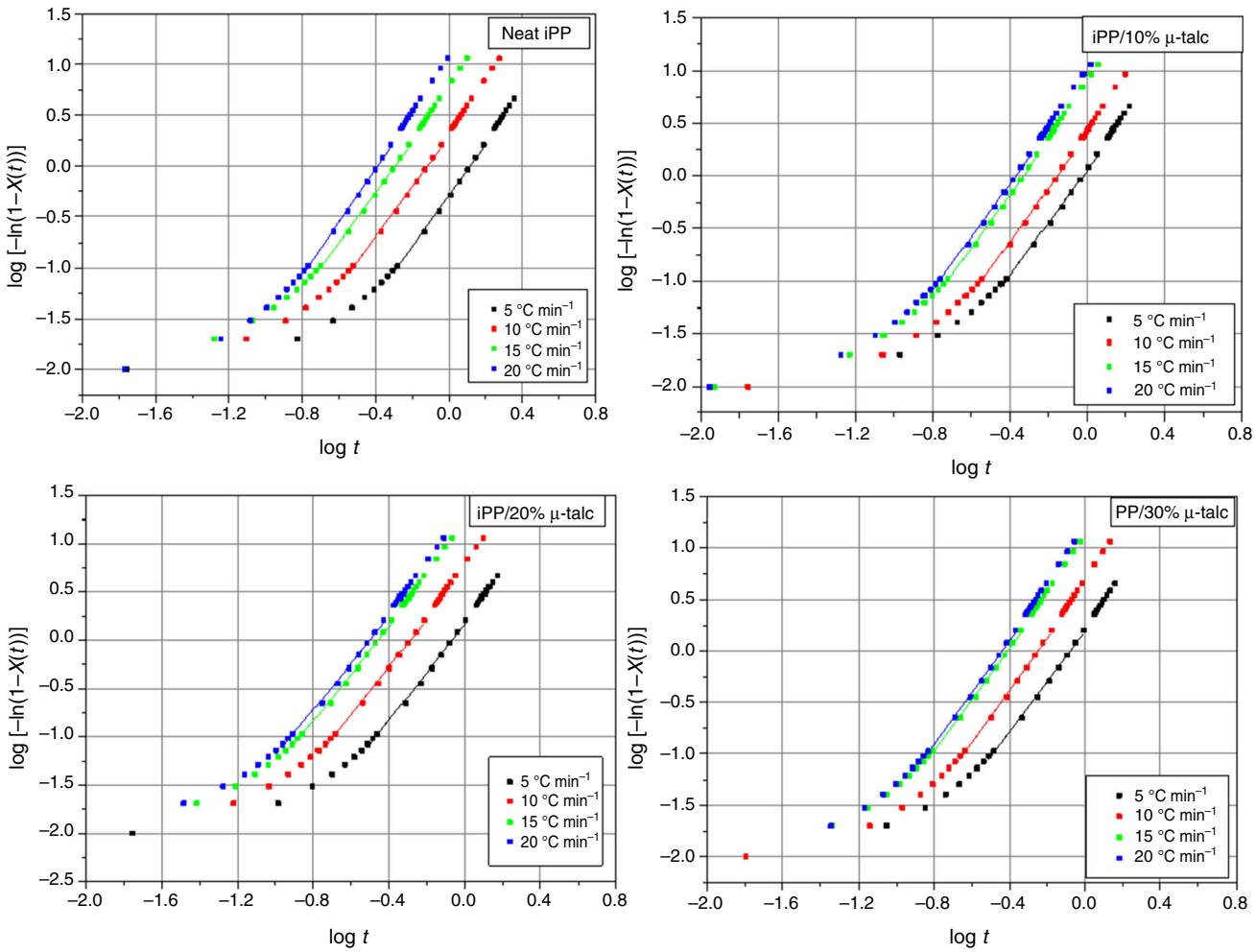

Fig. 6 Plot of log [− ln(1 − $X(t)$)] as a function of log t for neat iPP and iPP/μ-talc composites at different cooling rates

Mo's model

Mo and coll. [49–51] proposed a different kinetic model based on combining Avrami's and Ozawa's relations into the following forms

$$\log Z + n \log t = \log K(T) - m \log \mathrm{CR} \tag{6}$$

$$\log \mathrm{CR} = \log F(T) - \alpha \log t \tag{7}$$

where $F(T) = [K(T)/Z]^{1/m}$, and $K(T)$ and Z are constants of Ozawa's model and Jeziorny-modified Avrami's model, respectively. Mo's exponent is $\alpha = n/m$ where n and m are the Avrami's and Ozawa's exponents, respectively.

The kinetic constants calculated by Mo's method, log $F(T)$ and α are estimated, respectively, from the interception and the slope of the curve of log CR as a function of log t plotted in Fig. 8 and are reported in Table 4.

At a given crystallinity ratio, the $F(T)$ values of the various composites decrease in the following order: neat iPP > iPP/5% μ-talc > iPP/10% μ-talc > iPP/20% μ-talc, then increases for the iPP/30% μ-talc composite. This finding applies for any crystallinity ratio. This confirms that the presence of μ-talc improves the crystallization process of the iPP matrix [41]. For all samples the value of R^2 is very close to unity, i.e., a linear correlation between log CR and log t indicating that Mo's theory fairly well accounts for the NIC kinetics of neat iPP and its composites with μ-talc as well. However, a saturation effect of the crystallization activity can again be noticed from the decreasing value of $F(T)$ for μ-talc content FR > 20%.

Activation energy

The activation energy of crystallization is a useful means to quantify the efficacy of a filler in the crystallization process of polymer-based composites [54]. Kissinger [55] proposed an equation for calculating the activation energy for NIC as follows

$$\frac{\mathrm{d}\left[\ln\left(\mathrm{CR}/T_c^2\right)\right]}{\mathrm{d}(1/T_c)} = -\Delta E/R \tag{8}$$

Table 2 Jeziorny's parameters fitted for the NIC kinetics of neat iPP and iPP/μ-talc composites

Sample	CR/°C min^{-1}	Z_C	n	R^2
Neat iPP	5	0.87	2.48	0.997
	10	1.07	2.43	0.997
	15	1.11	2.43	0.997
	20	1.12	2.60	0.998
iPP/5% μ-talc	5	0.99	2.47	0.997
	10	1.09	2.48	0.997
	15	1.14	2.49	0.997
	20	1.11	2.43	0.997
iPP/10% μ-talc	5	1.02	2.47	0.997
	10	1.11	2.53	0.997
	15	1.15	2.53	0.998
	20	1.12	2.53	0.997
iPP/20% μ-talc	5	1.08	2.51	0.997
	10	1.18	2.49	0.997
	15	1.19	2.46	0.997
	20	1.15	2.43	0.996
iPP/30% μ-talc	5	1.09	2.44	0.996
	10	1.16	2.54	0.997
	15	1.17	2.49	0.997
	20	1.14	2.52	0.997

where ΔE is activation energy of crystallization, $R = 8.31$ J K^{-1} mol^{-1} is the gas constant and T_c is the peak temperature of the crystallization exotherm.

The Kissinger's relation can be transformed in the linear form

$$\ln(\mathrm{CR}/T_c^2) = (1/T_c)(-\Delta E/R) \tag{9}$$

The activation energy can be thus estimated from the slope of the ln (CR/T_c^2) curve as a function of $1/T_c$ according to Fig. 9. The values of the activation energy of NIC of neat iPP and the various composites are shown in Table 5. The decreasing value of ΔE with increasing μ-talc content confirms the benefiting role of the μ-talc particles on crystallization rate of the iPP matrix. However, the lower value of ΔE for the iPP/20% μ-talc composite confirms that the benefiting effect of μ-talc saturates for FR > 20% as observed from the above analyzes.

Nucleation activity

Dobreva and Gutzow [56, 57] proposed a simple determination method of the activity of substrates in the catalyzed nucleation of glass-forming melts. This approach can be applied to calculate the nucleation activity of a mineral filler, φ, on the crystallization process of a semicrystalline polymer matrix as defined by the following equation

$$\varphi = B^*/B \tag{10}$$

where B^* and B are the *heterogeneous* and *homogeneous* nucleation constants of the polymer matrix given by the following Eqs. (11) and (12), respectively,

$$\ln \varphi = c - B/\Delta T_c^2 \tag{11}$$

$$\ln \varphi = c - B^*/\Delta T_c^2 \tag{12}$$

The B and B^* constants are obtained from the slope of the plot of ln φ versus $1/\Delta T_c^2$, for neat iPP and composites, respectively, according to Fig. 10. Then φ is computed from Eq. (10) where $\Delta T_c = T_m - T_c$ is the undercooling with T_m the melting point. It is to be noticed that in this approach the nucleation step of neat iPP crystallization is assumed to be *homogeneous* so that Eq. (10) provides an evaluation of the *heterogeneous* nucleation effect of the filler in the composites compared to the own nucleation capability of the neat iPP matrix. In fact, the nucleation of neat semicrystalline polymers is generally *heterogeneous* due to catalysis residues and processing-induced impurities. Considering these remarks, data of the so-called μ-talc nucleation activity on the iPP matrix are reported in Table 6. Evidence is given that μ-talc behaves as an active nucleating agent. Moreover, it can be seen from Table 6 data that the iPP/20% μ-talc composite has a more effective nucleation effect than any of the other composites. This

Table 3 Parameters of Ozawa's method fitted for the NIC kinetics of neat iPP and iPP/μ-talc composites

T/°C	Neat iPP			iPP/5% μ-talc			iPP/10% μ-talc			iPP/20% μ-talc			iPP/30% μ-talc		
	Log $K(T)$	m	R^2	Log $K(T)$	m	R^2	Log $K(T)$	m	R^2	Log $K(T)$	m	R^2	Log $K(T)$	m	R^2
120	2.10	2.79	0.977	2.05	1.65	0.920	1.79	1.31	0.961	1.83	1.17	0.955	–	–	–
122	2.17	3.30	0.970	2.23	1.98	0.920	1.97	1.64	0.931	1.86	1.41	0.978	–	–	–
124	2.18	3.76	0.998	2.40	2.35	0.949	2.28	2.16	0.945	2.00	1.69	0.939	2.00	2.30	0.955
126	–	–	–	2.66	2.88	0.982	2.48	2.57	0.996	2.16	2.01	0.934	2.16	2.44	0.987
128	–	–	–	2.71	3.31	0.982	2.61	3.05	0.996	2.58	2.70	0.943	2.58	2.59	0.973
130	–	–	–	2.90	4.09	0.931	2.64	3.47	0.987	2.80	3.26	0.946	2.80	2.93	0.974

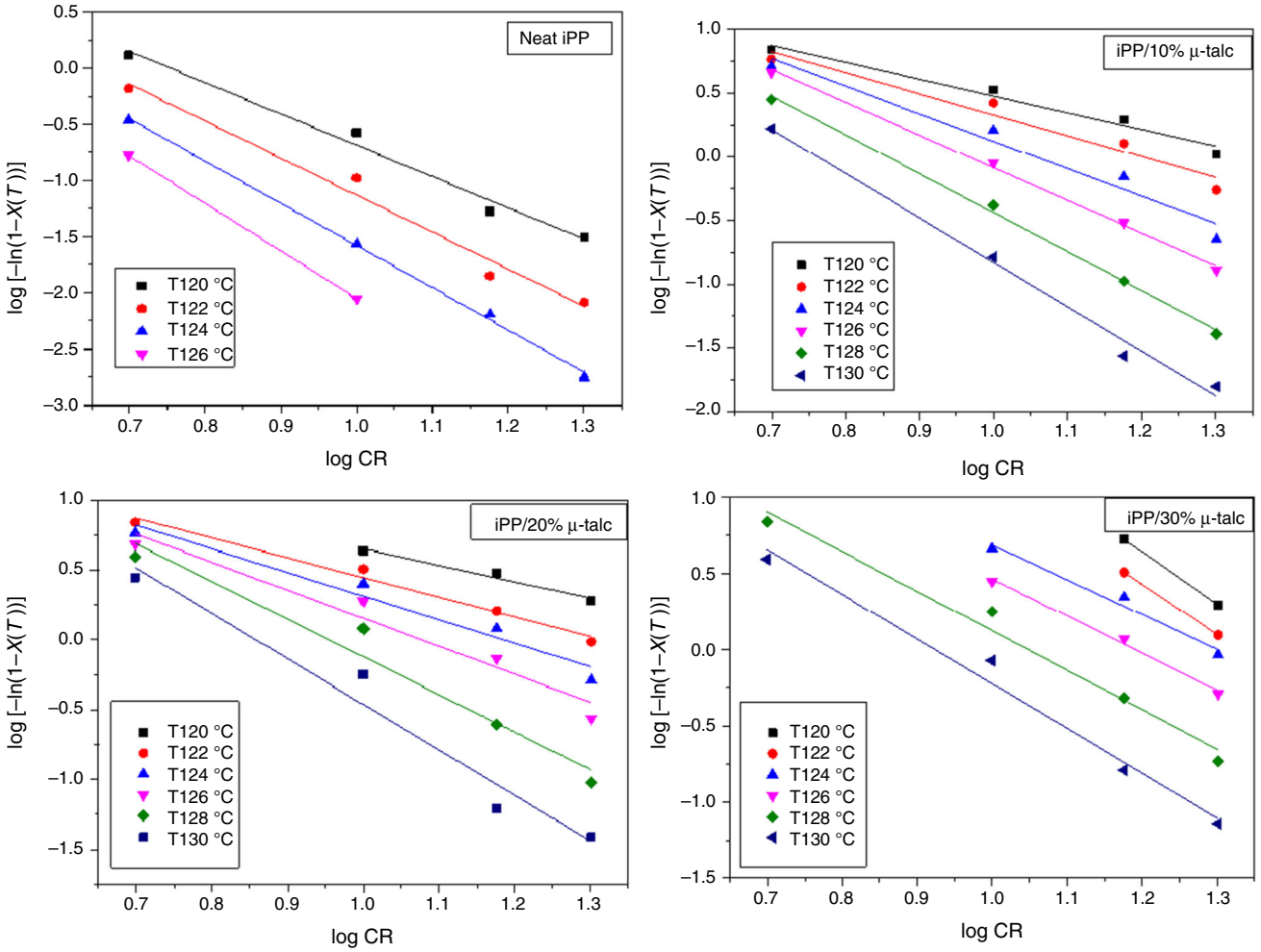

Fig. 7 Plot of log [− ln(1 − $X(t)$)] as a function of log CR for neat iPP and iPP/µ-talc composites at different temperatures

suggests that the reduced crystallization activity of µ-talc previously pointed out for FR > 20% actually has an origin in the nucleation step of the crystallization process.

This reduced nucleation effect of µ-talc for composites with FR> 20% is somewhat puzzling. An explanation can be put forward on the basis of the percolation process of filler particles dispersed in a polymer matrix. The mechanical aspect of this phenomenon for the present composites has been already discussed in a previous paper [40]. It is well known that percolation of nanometric particles of high form factor occurs at rather low filler content [58], typically a few % in volume as evidenced for amorphous polymer nanocomposites reinforced with cellulose whiskers of form factor close to 100. Indeed, as the crowding effect of the filler particles increases with increasing content in the composites, an impingement of the particles into each other gradually occurs accompanied with interparticle interactions resulting in a sudden increase in stiffness of the composites [58, 59]. However, in spite of the rather low form factor ≈ 5.5 of the µ-talc platelets in the present composites, mechanical percolation was shown to take place at a relatively low µ-talc content, namely FR ≈ 10% by mass, i.e., about 3% by volume [40]. This is due to the so-called *mixed* percolating network made of µ-talc platelets interconnected via iPP crystalline lamellae [40]. However, in the case of crystallization kinetics studied in this work, the actual impingement of the µ-talc particles into each other with increasing FR starts to occur beyond the threshold of *mixed* mechanical percolation accompanied with a mutual covering of the particles. This results in a gradual reduction of the surface of the µ-talc platelets actually available for nucleation of the iPP matrix. Moreover, the particles inter-distance gradually decreases with increasing FR which gradually disrupt the growth of the iPP crystalline lamellae. Both phenomena tend to hinder the development of the crystalline phase in the iPP matrix for FR > 20%. Notwithstanding the increase in µ-talc content beyond this later threshold enables the growth of additional iPP crystalline lamellae so that iPP crystallinity saturation only appears about FR ≈ 30% [41]. For

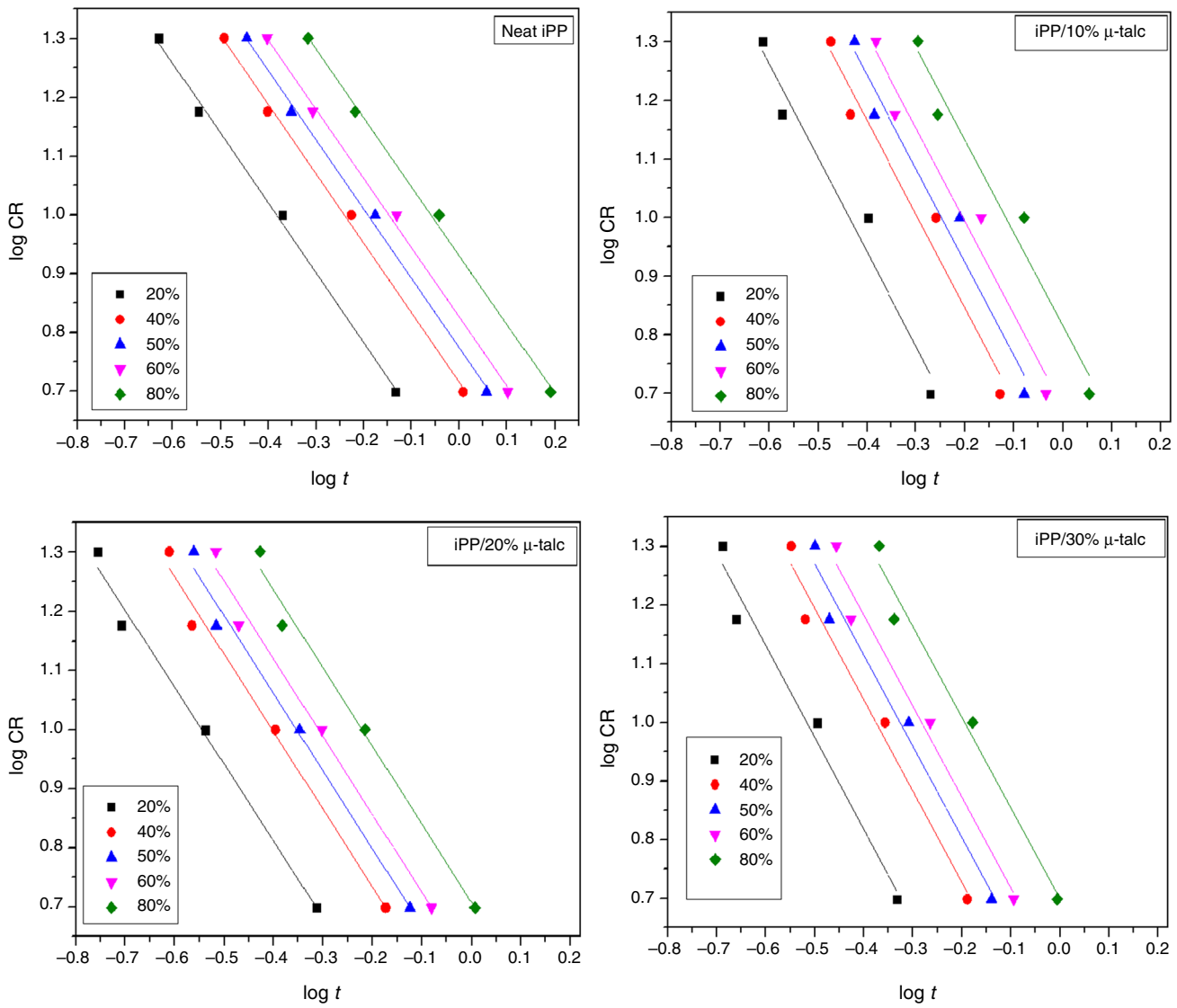

Fig. 8 Plot of log CR as a function of log *t* for neat iPP and iPP/μ-talc composites, for various % of transformation

Table 4 Parameters of Mo's model for the NIC kinetics of neat iPP and iPP/μ-talc composites

Xc/%	Neat iPP			iPP/5% μ-talc			iPP/10% μ-talc			iPP/20% μ-talc			iPP/30% μ-talc		
	$F(T)$	α	R^2	$F(T)$	α	R^2	$F(T)$	α	R^2	$F(T)$	α	R^2	$F(T)$	α	R^2
20%	3.51	1.19	0.995	2.40	1.37	0.981	1.99	1.61	0.947	1.55	1.57	0.984	1.96	1.30	0.965
40%	5.20	1.18	0.995	3.75	1.37	0.980	3.36	1.6	0.949	2.61	1.56	0.983	2.97	1.31	0.968
50%	5.95	1.18	0.995	4.38	1.37	0.980	4.03	1.59	0.949	3.11	1.55	0.983	3.43	1.31	0.969
60%	6.71	1.18	0.995	5.03	1.37	0.980	4.74	1.59	0.950	3.65	1.55	0.983	3.92	1.32	0.970
80%	8.52	1.17	0.995	6.65	1.38	0.979	6.54	1.59	0.951	5.00	1.55	0.983	5.11	1.32	0.971

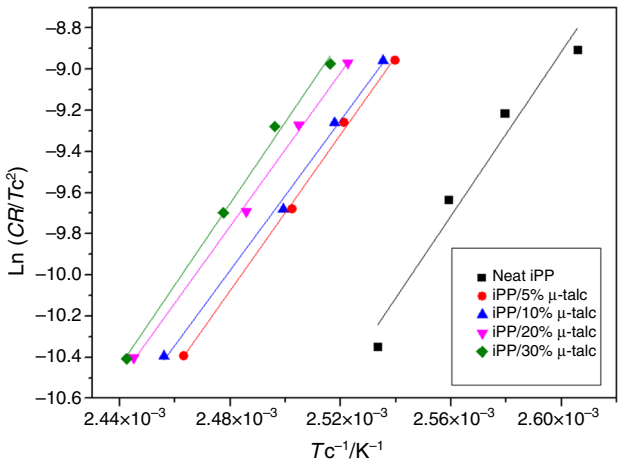

Fig. 9 Plot of ln (CR/T_c^2) versus $1/T_c$ for neat iPP and iPP/μ-talc composites

Table 5 Activation energy, ΔE, for the NIC kinetics of neat iPP and iPP/μ-talc composites

Sample	$-\Delta E$/kJ mol^{-1}
neat iPP	165
iPP/5% μ-talc	157
iPP/10% μ-talc	155
iPP/20% μ-talc	152
iPP/30% μ-talc	175

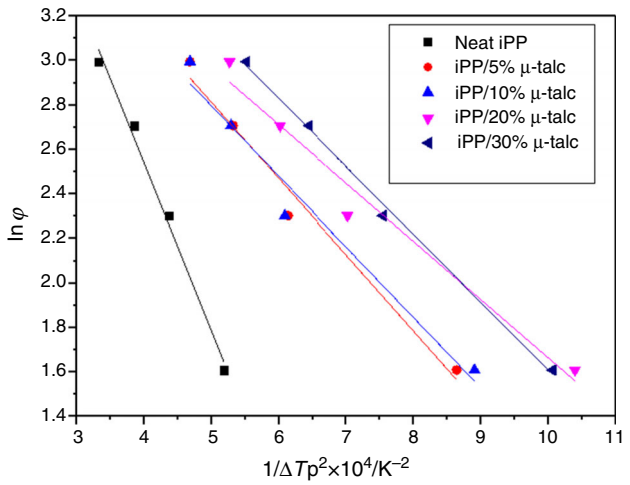

Fig. 10 Plot of ln φ as a function of $1/\Delta T_c^2$ for neat iPP and iPP/μ-talc composites

the sake of information, the saturation value of absolute crystallinity proved to be 0.60 ± 0.01 at CR = 5 °C min^{-1}. However, after the later study, crystallinity saturation strongly depends on cooling rate.

Table 6 Nucleation activity, φ, for the NIC kinetics of neat iPP and iPP/μ-talc composites

Sample	φ
Neat iPP	1
iPP/5% μ-talc	0.45
iPP/10% μ-talc	0.42
iPP/20% μ-talc	0.35
iPP/30% μ-talc	0.40

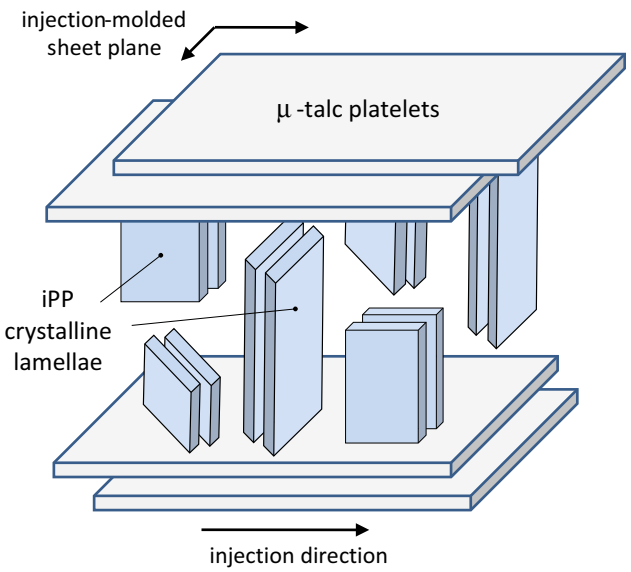

Fig. 11 Sketch of structural texturing of the iPP/μ-talc composites due to the nucleation of iPP crystalline lamellae onto the μ-talc platelets (the two components are not shown at the right scale for convenience; see text for details)

Concluding discussion

The NIC kinetics of iPP/μ-talc composites was analyzed in this study via Avrami's, Ozawa's and Mo's models, together with Kissinger's and Dobreva's approaches regarding the activation energy of crystallization and the nucleation activity, respectively.

Upon constant rate cooling, the peak crystallization temperature of the iPP matrix for all samples shifts to higher temperature with increasing content in μ-talc particles whereas the crystallization half-time decreases in parallel indicating a strong ability of μ-talc for improving the crystallization of the iPP matrix. All the theoretical crystallization approaches tested in this study more or less account for the crystallization kinetics of the iPP matrix and corroborate the favorable role of μ-talc on the crystallization kinetics. However, Mo's theory proved to be the best one to account for the NIC of neat iPP and its μ-talc/composites irrespective of the μ-talc content in the composites. It is worth noticing that similar findings have been already reported by several authors for various

polymer-based composites [34, 49–51, 60–63]. This study thus reinforces the relevance of Mo's approach.

The $F(T)$ function of Mo's theory decreases with the addition of μ-talc which quantitatively confirms that this kind of filler improves the crystallization of the iPP matrix in the composites. This finding supports the conclusion of previous studies suggesting a specific nucleation activity of talc irrespective of its particle size and form factor (see Introduction section). This nucleation effects are responsible for the crystalline texturing of the iPP matrix as evidenced from Fig. 1. Indeed, the nucleation role of the μ-talc platelets involves a growth of iPP crystalline lamellae roughly normal to the μ-talc platelets surface probably due to a so-called epitaxial nucleation process [64, 65]. The sketch of Fig. 11 shows iPP crystalline lamellae growing down from the μ-talc platelets above as well as iPP lamellae growing up from the platelets below. The drawing of pairs of iPP crystalline lamellae holds for the buildup of lamella stackings instead of individual lamellae. Then considering that the μ-talc platelets exhibit a strong shear-induced orientation parallel to the plane of the sheets consecutive to the injection-molding process [40], Fig. 11 shows up that the iPP lamellae should display an orientation normal to the sheet plane, which is actually observed in Fig. 1.

However, at a given crystallinity X_c, and whatever the X_c value, the $F(T)$ function of the iPP matrix exhibits a minimum value for the composite with μ-talc content FR $\approx$ 20%. This indicates an optimum effect of μ-talc on the iPP crystallization for this composition. In addition to this evolution of Mo's function with μ-talc content, both the activation energy and the nucleation activity exhibit minimum values for the iPP composite with μ-talc content FR $\approx$ 20%. This similar evolution of the last two parameters gives evidence that the improvement of the iPP matrix crystallization by μ-talc actually relies on nucleation grounds.

The reduced nucleation effect for composite with μ-talc content FR$\geq$ 20% has been given an explanation in relation to previous specific findings regarding the same composites. Indeed, the observation from a former study of a mechanical percolation that saturates at FR $\approx$ 10% is relevant to the buildup of a stiff structural continuity between the μ-talc platelets and the iPP crystalline lamellae. The present observation of a nucleation optimum at FR $\approx$ 20% can be attributed to the increase in crowding effect of the μ-talc platelets that gradually impinge into each other and mutually cover each other with increasing content so that only a part of their surface remains fully active for crystal nucleation. In parallel, the observation from a recent structural study that the iPP matrix crystallinity gradually saturates at a μ-talc content FR$\approx$ 30% is most probably due to the fact that the increasing number of μ-talc particles is able to compensate—to some extent—the reduced nucleation activity of the μ-talc particles in the range 20 < FR < 30%. Then, only when FR> 30% the overall crystallinity of the iPP matrix is actually impacted by the reduction of μ-talc nucleation activity, in conjunction with the intrinsic crystallization capability of iPP upon quiescent conditions.

To sum up, the structural and mechanical behavior of iPP/μ-talc composites obey the following features in relation to μ-talc concentration: FR $\approx$ 10% is the saturation threshold of mixed mechanical percolation network of μ-talc platelets and iPP crystalline lamellae; FR $\approx$ 20% generates the optimum nucleation effect of μ-talc on the crystallization of the iPP matrix; FR $\approx$ 30% is the μ-talc limiting concentration for optimum crystallinity of the iPP matrix.

Acknowledgements The authors are indebted to Multibase/Dow Corning (Saint-Laurent-du-Pont, France) for supplying the injection-molded samples and data on the processing conditions and physico-chemical characteristics as well. Dr. P. Prèle from Multibase is particularly acknowledged for fruitful comments.

References

1. Karger-Kocsis J, editor. Polypropylene: an A-Z reference. Dordrecht: Springer Science Business; 1999.
2. Karger-Kocsis J, editor. Polypropylene: structure, blends and composites; Vol. 3: composites. London: Chapman and Hall; 1994.
3. Rothon RN, editor. Particulate-filled polymer composites. 2nd ed. Shrewsbury: Rapra Technology Ltd.; 2002.
4. Oya A, Kurokawa Y, Yasuda H. Factors controlling mechanical properties of clay mineral/polypropylene nanocomposites. J Mater Sci. 2000;35:1045–50.
5. Bakis CE, Bank LC, Brown VL, Cosenza E, Davalos JF, Lesko JJ, Machida A, Rizkalla SH, Triantafillou TC. Fiber-reinforced polymer composites for construction—state of the art—review. J Compos Constr. 2002;6:73–87.
6. Hussain F, Hojjati M, Okamoto M, Gorga RE. Polymer-matrix nanocomposites, processing, manufacturing, and application: an overview. J Compos Mater. 2006;40:1511–75.
7. Százdi L, Pozsgay A, Pukánszky B. Factors and processes influencing the reinforcing effect of layered silicates in polymer nanocomposites. Eur Polym J. 2007;43:345–59.
8. Arroyo M, Lopez-Manchado MA, Avalos F. Crystallization kinetics of polypropylene: II. Effect of the addition of short glass fibres. Polymer. 1997;38:5587–93.
9. Thomason JL. The influence of fibre length and concentration on the properties of glass fibre reinforced polypropylene. The properties of injection moulded long fibre PP at high fibre content. Compos Part A Appl Sci Manuf. 2005;36:995–1003.
10. Cui L, Wang P, Zhang Y, Zhou X, Xu L, Zhang L, Guo X. Glass fiber reinforced and β-nucleating agents regulated polypropylene: a complementary approach and a case study. J Appl Polym Sci. 2018;135:45768.
11. McGenity PM, Hooper JJ, Paynter CD, Riley AM, Nutbeem C, Elton NJ, Adams JM. Nucleation and crystallization of polypropylene by mineral fillers: relationship to impact strength. Polymer. 1992;33:5215–24.

12. Gonzalez A, de Saja JA, Alonso M. Morphology and tensile properties of compression-moulded talc-filled polypropylene. Plast Rubber Compos Proc Appl. 1995;3:131–7.
13. Leong YW, Abu Bakar MB, Ishak ZAM. Comparison of the mechanical properties and interfacial interactions between talc, kaolin, and calcium carbonate filled polypropylene composites. J Appl Polym Sci. 2004;91:3315–26.
14. Weon JI, Sue HJ. Mechanical properties of talc- and $CaCO_3$-reinforced high-crystallinity polypropylene composites. J Mater Sci. 2006;41:2291–300.
15. Abu Bakar MB, Leong YW, Ariffin A, Ishak ZAM. Mechanical, flow and morphological properties of talc- and kaolin-filled polypropylene hybrid composites. J Appl Polym Sci. 2007;104:434–41.
16. Fujiyama M, Wakino T. Crystal orientation in injection molding of talc-filled polypropylene. J Appl Polym Sci. 1991;42:9–20.
17. Maiti SN, Sharma KK. Studies on polypropylene composites filled with talc particles. J Mater Sci. 1992;27:4605–13.
18. Guerrica-Echevarria G, Eguiazabal JI, Nazabal J. Effects of reprocessing conditions on the properties of unfilled and talc-filled polypropylene. Polym Degrad Stabil. 1996;53:1–8.
19. Fujiyama M. Crystal orientation in injection moldings of talc-filled polyolefins. Int Polym Proc. 1998;13:284–90.
20. Naiki M, Fukui Y, Matsumura T, Nomura T, Matsuda M. The effect of talc on the crystallization of isotactic polypropylene. J Appl Polym Sci. 2001;79:1693–703.
21. Choi WJ, Kim SC. Effects of talc orientation and non-isothermal crystallization rate on crystal orientation of polypropylene in injection-molded polypropylene/ethylene–propylene rubber/talc blends. Polymer. 2004;45:2393–401.
22. Rotzinger B. Talc-filled PP: a new concept to maintain long term heat stability. Polym Degrad Stabil. 2006;91:2884–7.
23. Zhou X-P, Xie X-L, Yu Z-Z, Mai Y-W. Intercalated structure of polypropylene/in situ polymerization-modified talc composites via melt compounding. Polymer. 2007;48:3555–64.
24. Branciforti MC, Oliveira CA, de Sousa JA. Molecular orientation, crystallinity, and flexural modulus correlations in injection molded polypropylene/talc composites. Polym Adv Technol. 2010;21:322–30.
25. Castillo LA, Barbosa SE, Capiati NJ. Surface-modified talc particles by acetoxy groups grafting: effects on mechanical properties of polypropylene/talc composites. Polym Eng Sci. 2013;53:89–95.
26. Alexandre M, Dubois P. Polymer-layered silicate nanocomposites: preparation, properties and uses of a new class of materials. Mater Sci Eng Rep. 2000;28:1–63.
27. Kotal M, Bhowmick AK. Polymer nanocomposites from modified clays: recent advances and challenges. Prog Polym Sci. 2015;51:127–87.
28. Vermogen A, Masenelli-Varlot K, Seguela R, Duchet-Rumeau J, Boucard S, Prele P. Evaluation of the structure and dispersion in polymer-layered silicate nanocomposites. Macromolecules. 2005;38:9661–9.
29. Wang LM. Preparation and characterization of polypropylene/clay nanocomposites. Appl Mech Mater. 2011;55:1584–7.
30. Zhu S, Chen J, Zuo Y, Li H, Cao Y. Montmorillonite/polypropylene nanocomposites: mechanical properties, crystallization and rheological behaviors. Appl Clay Sci. 2011;52:171–8.
31. Levita G, Marchetti A, Lazzeri A. Fracture of ultrafine calcium carbonate/polypropylene composites. Polym Compos. 1989;10:39–43.
32. Mareri P, Bastide S, Binda N, Crespy A. Mechanical behaviour of polypropylene composites containing fine mineral filler: effect of filler surface treatment. Compos Sci Technol. 1998;58:747–52.
33. Cayer-Barrioz J, Ferry L, Frihi D, Cavalier K, Seguela R, Vigier G. Microstructure and mechanical behavior of polyamide 66-precipitated calcium carbonate composites: influence of the particle surface treatment. J Appl Polym Sci. 2006;100:989–99.
34. Huang Y, Chen G, Yao Z, Li H, Wu Y. Non-isothermal crystallization behavior of polypropylene with nucleating agents and nano-calcium carbonate patrticles. Eur Polym J. 2005;41:2753–60.
35. Yang K, Yang Q, Li G, Sun Y, Feng D. Morphology and mechanical properties of polypropylene/calcium carbonate nanocomposites. Mater Lett. 2006;60:805–9.
36. Jiang L, Zhang J, Wolcott MP. Comparison of polylactide/nano-sized calcium carbonate and polylactide/montmorillonite composites: reinforcing effects and toughening mechanisms. Polymer. 2007;48:7632–44.
37. Gahleitner M, Grein C, Bernreitner K. Synergistic mechanical effects of calcite micro- and nanoparticles and β-nucleation in polypropylene copolymers. Eur Polym J. 2012;48:49–59.
38. Fernando NAS, Thomas NL. Investigation of precipitated calcium carbonate as a processing aid and impact modifier in poly(vinyl chloride). Polym Eng Sci. 2012;52:2369–74.
39. Ferrage E, Martin F, Boudet A, Petit S, Fourty G, Jouffret F, Ferret J. Talc as nucleating agent of polypropylene: morphology induced by lamellar particles addition and interface mineral-matrix modelization. J Mater Sci. 2002;37:1561–73.
40. Frihi D, Masenelli-Varlot K, Vigier G, Satha H. Mixed percolating network and mechanical properties of polypropylene/talc composites. J Appl Polym Sci. 2009;145:3097–105.
41. Makhlouf A, Satha H, Frihi D, Gherib S, Seguela R. Optimization of the crystallinity of polypropylene/submicronic-talc composites: the role of filler ratio and cooling rate. Express Polym Lett. 2016;10:237–47.
42. Fornes DT, Paul DR. Crystallization behavior of nylon6 nanocomposites. Polymer. 2003;44:3945–61.
43. Lincoln DM, Vaia RA, Wang Z-G, Hsiao BS. Secondary structure and elevated temperature crystallite morphology of nylon-6/layered silicate nanocomposites. Polymer. 2001;42:1621–31.
44. Avrami M. Kinetics of phase change. I. General theory. J Chem Phys. 1939;7:1103–12.
45. Avrami M. Kinetics of phase change. II. Transformation-time relations for random distribution of nuclei. J Chem Phys. 1940;8:212–24.
46. Jeziorny A. Parameters characterizing the kinetics of the non-isothermal crystallization of poly(ethylene-terephthalate) determined by DSC. Polymer. 1978;19:1142–4.
47. Durmus A, Yalçinyuva T. Effects of additives on non-isothermal crystallization kinetics and morphology of isotactic polypropylene. J Polym Res. 2009;16:489–98.
48. Ozawa T. Kinetics of non-isothermal crystallization. Polymer. 1971;12:150–8.
49. Liu TX, Mo ZS, Zhang HF. Non-isothermal crystallization behavior of a novel poly(aryl ether ketone): PEDEKmK. J Appl Polym Sci. 1998;67:815–21.
50. Liu SY, Yu YG, Cui Y, Zhang HF, Mo ZS. Isothermal and non-isothermal crystallization kinetics of nylon11. J Appl Polym Sci. 1998;70:2371–80.
51. Liu TX, Mo ZS, Wang SG, Zhang HF. Non-isothermal melt & cold crystallization kinetics of poly(ary1-ether-ether-ketone-ketone). Polym Eng Sci. 1997;37:568–75.
52. Labour T, Gauthier C, Seguela R, Vigier G, Bomal Y, Orange G. Influence of the β crystalline phase on the mechanical properties of unfilled and $CaCO_3$-filled polypropylene. I. Structural and mechanical characterization. Polymer. 2001;42:7127–35.
53. Grein C. Toughness of neat, rubber-modified and filled β-nucleated polypropylene: from fundamentals to applications. Adv Polym Sci. 2005;188:43–104.

54. Ariffin A, Ariff ZM, Jikan SS. Evaluation on non-isothermal crystallization kinetics of polypropylene/kaolin composites by employing Dobreva and Kissinger methods. J Therm Anal Calorim. 2011;103:171–7.
55. Kissinger HE. Variation of peak temperature with heating rate in differential thermal analysis. J Res Nat Bur Stand. 1956;57:217–21.
56. Dobreva A, Gutzow I. Activity of substrates in the catalyzed nucleation of glass-forming melts. I. Theory. J Non-Cryst Solids. 1993;162:1–12.
57. Dobreva A, Gutzow I. Activity of substrates in the catalyzed nucleation of glass-forming melts. II. Experimental evidence. J Non-Cryst Solids. 1993;162:13–25.
58. Favier V, Chanzy H, Cavaille J-Y. Polymer nanocomposites reinforced by cellulose whiskers. Macromolecules. 1996;28:6365–7.
59. Sengupta R, Bhattacharya M, Bandyopadhyay S, Bhowmick AK. A review on the mechanical and electrical properties of graphite and modified graphite reinforced polymer composites. Prog Polym Sci. 2011;36:638–70.
60. Saengsuwan S, Tongkasee P, Sudyoadsuk T, Promarak V, Keawin T, Jungsuttiwong S. Non-isothermal crystallization kinetics and thermal stability of the in situ reinforcing composite films based on thermotropic liquid crystalline polymer and polypropylene. J Therm Anal Calorim. 2011;103:1017–26.
61. Shi YH, Dou Q. Non-isothermal crystallization kinetics of β-nucleated isotactic polypropylene. J Therm Anal Calorim. 2013;112:901–11.
62. Dai X, Zhang Z, Chen C, Li M, Tan Y, Mai K. Non-isothermal crystallization kinetics of montmorillonite filled β-isotactic polypropylene nanocomposites. J Therm Anal Calorim. 2015;121:829–38.
63. Layachi A, Frihi D, Satha H, Seguela R, Gherib S. Non-isothermal crystallization kinetics of polyamide 66/glass fibers/carbon black composites. J Therm Anal Calorim. 2016;124:1319–29.
64. Fillon B, Lotz B, Thierry A, Wittmann J-C. Self-nucleation and enhanced nucleation of polymers. Definition of a convenient calorimetric "efficiency scale" and evaluation of nucleating additives in isotactic polypropylene (α-phase). J Polym Sci Polym Phys. 1993;31:1395–405.
65. Mathieu C, Thierry A, Wittmann J-C, Lotz B. Specificity and versatility of nucleating agents toward isotactic polypropylene crystal phases. J Polym Sci Polym Phys. 2002;40:2504–15.